Natural Hazards **27:** 15–33, 2002.

The $M_w = 6.0$, 7 September 1999 Athens Earthquake

P. PAPADIMITRIOU, N. VOULGARIS, I. KASSARAS, G. KAVIRIS, N. DELIBASIS and K. MAKROPOULOS
Department of Geophysics, University of Athens, 157 84 Athens, Greece

Received: 22 August 2000; accepted in revised form 8 February 2002

Abstract. On 7 September 1999 at 11:56 GMT a destructive earthquake ($M_w = 6.0$) occurred close to Athens (Greece). The rupture process is examined using data from the Cornet local permanent network, as well as teleseismic recordings. Data recorded by a temporary seismological network were analyzed to study the aftershock sequence. The mainshock was relocated at 38.105°N, 23.565°E, about 20 km northwest of Athens. Four foreshocks were also relocated close to the mainshock. The modeling of teleseismic P and SH waves provides a well-constrained focal mechanism of the mainshock (strike = 105°, dip = 55° and rake = $-80°$) at a depth of 8 km and a seismic moment $M_0 = 1.010^{25}$ dyn·cm. The obtained fault plane solution represents normal faulting indicating an almost north-south extension. More than 3500 aftershocks were located, 1813 of which present RMS < 0.1 s and ERH, ERZ < 1.0 km. Two main clusters were distinguished, while the depth distribution is concentrated between 2 and 11 km. Over 1000 fault plane solutions of aftershocks were constrained, the majority of which also correspond to N–S extension. No surface breaks were observed but the fault plane solution of the mainshock is in agreement with the tectonics of the area and with the focal mechanisms obtained by aftershocks. The hypocenter of the mainshock is located on the deep western edge of the fault plane. The relocated epicenter coincides with the fringe that represents the highest deformation observed on the differential interferometric image. The calculated source duration is 5 sec, while the estimated dimensions of the fault are 15 km length and 10 km width. The source process is characterized by unilateral eastward rupture propagation, towards the city of Athens. An evident stop phase observed in the recordings of the Cornet local stations is interpreted as a barrier caused by the Aegaleo Mountain.

Key words: Athens earthquake, synthetic seismograms, fault plane solution, source directivity, aftershocks, interferogram.

1. Introduction

An important earthquake ($M_w = 6.0$) occurred on 7 September 1999 at a distance of about 20 km from the center of the city of Athens, the capital of Greece (Figure 1). The epicenter is located south of the mountain Parnitha, close to the Saronikos Gulf. This event was the strongest in an area that was until now considered as one of low seismic activity, since no important earthquakes were reported neither by historical catalogues, nor during the instrumental period. Therefore, this area was considered to be of low seismic hazard. Although the earthquake magnitude was

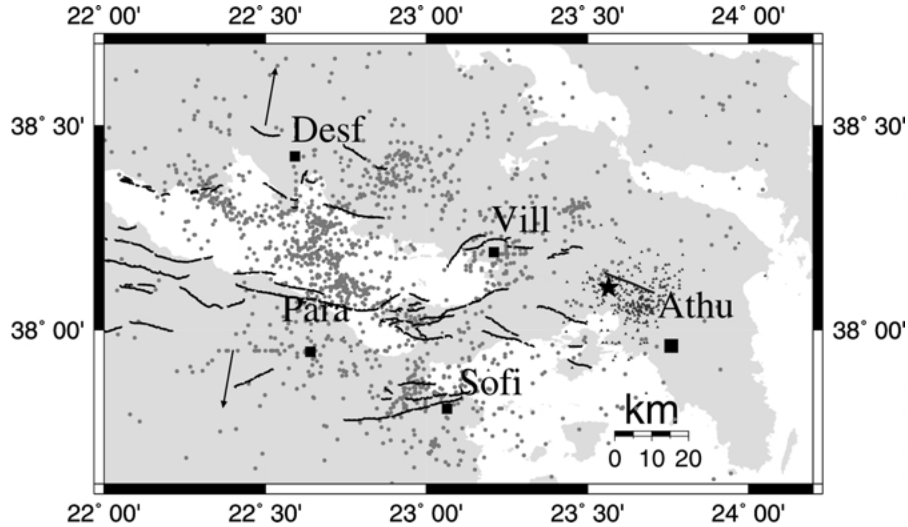

Figure 1. Best located events by Cornet network for 1996–1998 (circles) and aftershock activity of the 7 September 1999 Athens earthquake (triangles). The star represents the epicenter of the mainshock. The squares represent the stations of the Cornet network. Active faults around the Gulf of Corinth are plotted and the arrows present the direction of extension of the Gulf of Corinth.

moderate, the damage was very serious, since the intensity reached IX. One hundred and forty-three people were killed, a great number were wounded and several thousands of people became homeless. Over a hundred buildings collapsed or were totally destroyed and thousands sustained considerable damage. Consequently it may be considered as one of the most disastrous earthquakes that occurred in Greece during the last centuries.

The seismogenic area is situated next to the eastern edge of the Gulf of Corinth, where important earthquakes occurred during the last decades (Papadimitriou *et al*., 1994; Hatzfeld *et al*., 1996; Bernard *et al*., 1997). The Gulf of Corinth is characterized by E–W trending, north-dipping normal faulting and by NNE–SSW direction of extension with a rate of about 1 cm/yr (Armijo *et al*., 1996; Rigo *et al*., 1996). In 1981 three major earthquakes occurred at the easternmost part of the Gulf with magnitudes $M_S = 6.7$, 6.4 and 6.4 (Jackson *et al*., 1982; Papazachos *et al*., 1984; King *et al*., 1985). The focal mechanisms calculated for these events revealed normal faulting trending E–W, dipping north for the two first events and south for the last event of 4 March. The focal depths that were determined vary between 8 and 10 km. Surface breaks that were related to the second and the third event were observed. The maximum coseismic slip was 150 cm, but the more typical range was 50–70 cm. The aftershock activity was mainly concentrated around the eastern edge of the Gulf and close to the Vill station (Figure 1).

The Cornet seismological permanent network that consists of four stations has been installed since 1995 around the eastern Gulf of Corinth by the Department of

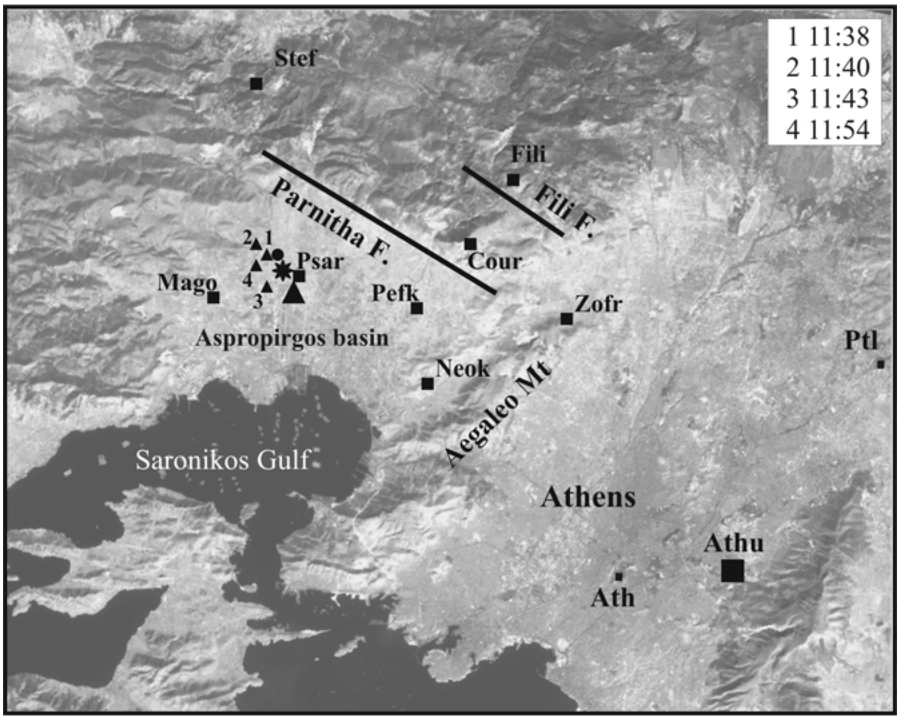

Figure 2. The initial (big triangle) and relocated epicenters (star) of the mainshock are shown. Small triangles represent the relocated foreshocks and the circle the epicenter of the master aftershock. Small squares represent the location of the stations of the temporary local network and two permanent NOA stations. Main faults of the area are also indicated.

Geophysics of the University of Athens (Papadimitriou *et al.*, 1996). For the period 1996–1999 approximately 5000 events were recorded, while more than 2000 were located in the Gulf and the surrounding area. Selected events are presented in Figure 1. Nevertheless, no clear evidence of seismic activity was observed in the vicinity of the Parnitha fault during the operation period of the Cornet network, until the earthquake sequence of September 1999. Four foreshocks, the mainshock and numerous aftershocks were recorded by the Cornet network. In addition, a temporary network that consisted of 6 digital 3-component REFTEK seismographs (Fili, Stef, Mago, Psar, Neok and Zofr) and of two strong motion digital instruments (Pefk and Cour) was installed 1 day after the occurrence of the mainshock, to record the aftershock activity in the area. The station locations are shown in Figure 2.

In this paper results obtained by seismological data from the local Cornet network, the worldwide network (GSN) and the temporary seismological network following the 7 September 1999 Athens earthquake are analyzed. The mainshock was relocated and the source parameters were determined using body wave modeling. Following, seismological data and tectonic observations were combined in

Table I. Locations and magnitudes of the mainshock reported by different institutes

Date	Time	Latitude (°) N	Longitude	Depth (°) E	M_S (km)	M_w	Institute
99-09-07	11:56:50.8	38.105	23.565	8		6.0	ATHU
	11:56:50.5	38.15	23.62	30	5.9		NOA
	11:56:49.3	38.132	23.545	10	5.6	5.9	USGS
	11:56:49.3	38.119	23.605	10	5.8	6.0	PDE
	11:56:49.4	38.120	23.600	10		6.0	HRV

order to study the characteristics and the geometry of the fault zone, as well as the rupture process of the earthquake.

2. Relocation of the Mainshock

The Aspropirgos basin is bordered to the north by the southern slopes of the mountain Parnitha characterized by normal faulting striking E–W and dipping south. The length of this fault, visible in aerial photographs and satellite images, is of the order of 15 km. To the east it is bordered by the Aegaleo Mountain characterized by transverse limestone ridges striking N–S, while to the south it is delimited by the Saronikos Gulf. The mainshock occurred on 7 September 1999 in the Aspropirgos basin on the Parnitha fault and was preceded by four foreshocks of magnitudes $M_D = 3.7$, 3.0, 3.4 and 3.6, which occurred within a time span of 18 min (the first 18 min and the last 2 min) before the mainshock (Figure 2). The location of the mainshock reported by different seismological institutes varies significantly (Table I). Thus, the relocation of the foreshocks and of the mainshock is necessary for the interpretation of the rupture process.

In order to relocate the mainshock and the foreshocks, an aftershock recorded both by the Cornet and the temporary seismological network is selected as a master event. The master event, that is well located, was used to estimate systematic delays for the first arrivals at the Cornet stations. Arrival times from two stations of the National Observatory of Athens (NOA) permanent seismological network (ATH and PTL) were also used (Figure 2). We ran several times the HYPO71 program with various weights to the stations and with or without the arrival times of the NOA stations. The obtained hypocenter locations were very stable, clustered within less than 1 km around 38.105°N, 23.565°E with an RMS of 0.30 s. The relocated epicenter of the mainshock is very close to the initial location obtained using data only by the Cornet network, to the USGS epicenter and to the relocated one (38.08°, 23.58°) proposed by Papadopoulos *et al.* (2000). On the other hand, it is significantly different from the epicenters proposed by NOA, PDE and HRV that are shifted about 10 km to the east. The same procedure was followed for the

Table II. Source parameters determination by different institutes

Azimuth (°)	Dip (°)	Rake (°)	Scalar moment (dyn cm)	Institute
105	55	–80	1.0 10^{25}	ATHU
123	55	–84	7.8 10^{24}	USGS
116	39	–81	1.1 10^{25}	HRV

four foreshocks that were relocated very close to the mainshock and the results are presented in Figure 2. The obtained solutions suggest that the hypocenters of the mainshock and of the foreshocks are located at the deep western edge of the fault plane.

3. Teleseismic body-wave modeling

In order to calculate the source parameters of the mainshock we used forward modeling (Papadimitriou *et al.*, 2000). For this purpose, broadband teleseismic recordings from IRIS-DMC and ORFEUS were collected and those at epicentral distances between 30° and 90° were selected. The records were first deconvolved from the instrumental response and integrated to obtain displacement. Next, the data were filtered using a band-pass Butterworth filter with cutoff frequencies at 0.1 Hz and 1.0 Hz. The anelastic attenuation along the path is applied with a ratio of travel time to average quality factor of 1 sec and 4 sec for P and SH waves, respectively. We inverted a 10-sec time window from the seismograms.

We assumed a simple point source and inverted the P and SH waveforms at all the selected stations in order to determine the source parameters. The final best-fit solution is: $\phi = 105°$, $\delta = 55°$, $\lambda = -80°$, depth H = 8.0 km and seismic moment $M_0 = 1.010^{25}$ dyn·cm. Initially, we used a simple trapezoid source time function of 5 sec duration and the fit between the synthetic and the observed waveforms was satisfactory. Nevertheless, this fit was ameliorated by introducing a complex source time function that was calculated using an inversion technique (Kikuchi and Kanamori, 1982), where the focal mechanism and the centroid depth were fixed, taking into account the result of this study (Figure 3a, b). The source parameters determined in this study and those proposed by other institutes, also obtained by modeling, are presented in Table II. The results are comparable indicating normal faulting striking approximately E–W. The main differences concern the strike and the dip of the fault. The azimuth calculated in the present study is closer to E–W, while the value of the dip given by HRV is smaller. The values of azimuth and dip were calculated using mainly the recordings from FURI, KMBO and BGCA teleseismic stations, since they are very close to the fault plane dipping south.

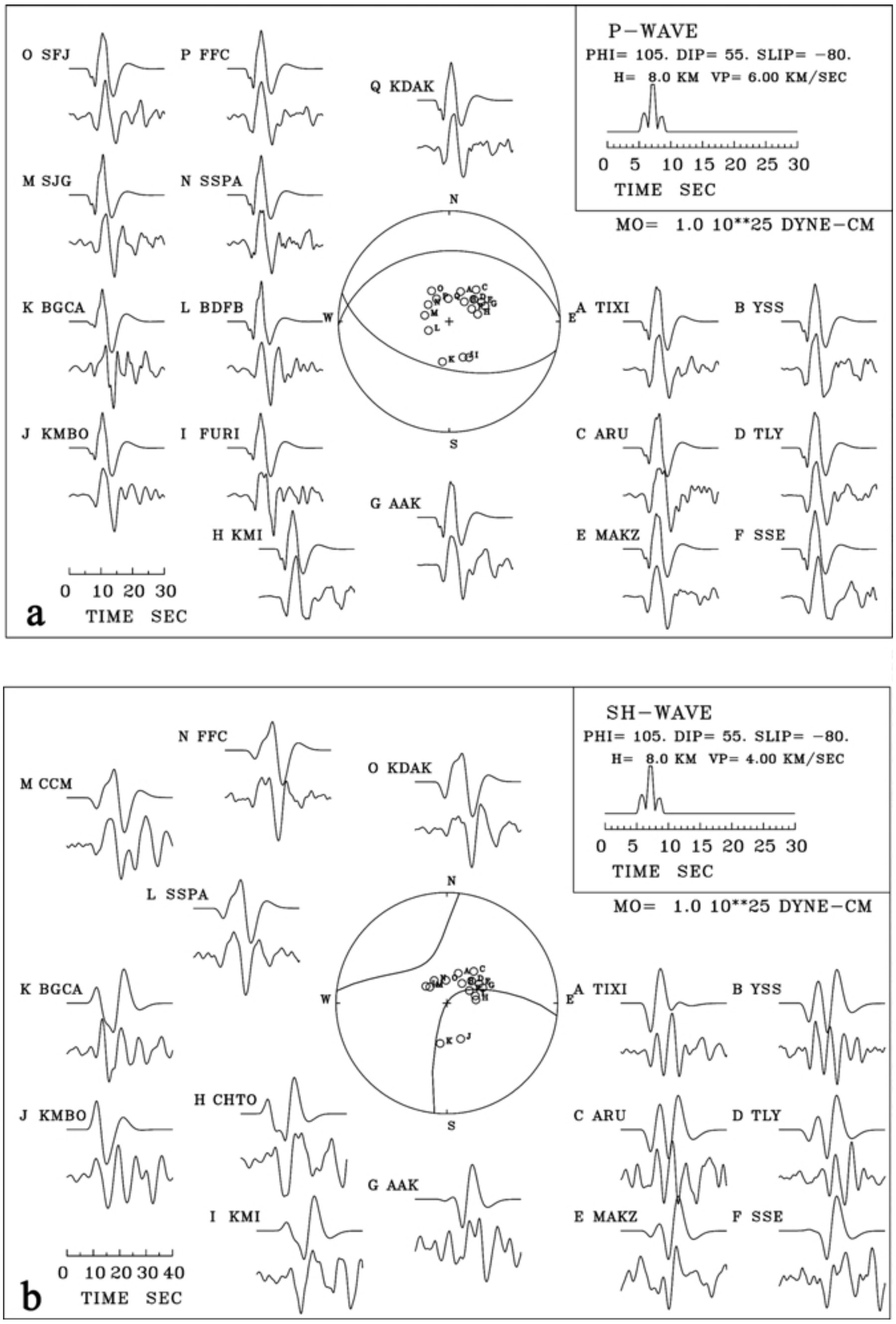

Figure 3. Body-wave modeling of the P (a) and the SH (b) teleseismic waves. The best-fit solution of the focal mechanism, the depth, the source time function and the seismic moment are presented.

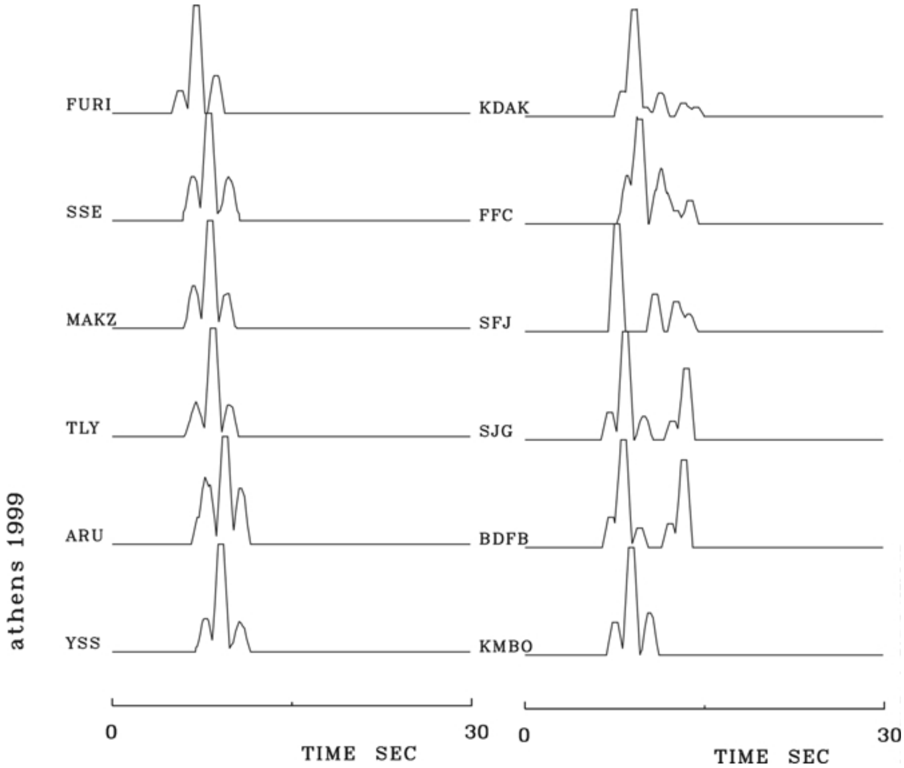

Figure 4. Source time functions from P-wave inversion for selected teleseismic stations.

The complexity of the source time function was calculated for each teleseismic station using the above mentioned inversion technique. Since their number is large and most of them cover similar azimuths, the most representative examples are presented in Figure 4. The shape of the source time function is almost similar for all the stations, showing it can be decomposed in three elementary sources. Comparing the duration of the source time function we observe that it is longer in some stations (e.g., BDFB, SJG the SFJ) located to the west and shorter in some other stations (e.g., MAKZ, SSE, FURI and KMBO) located to the east. This difference could be attributed as a directivity effect of the source propagation.

A differential interferogram showing the surface deformation (Figure 5) was produced using two SAR images taken on 15 July and 23 September 1999, respectively (this interferogram has been kindly offered by EPPO). The altitude ambiguity of the interferogram, that was obtained using a digital elevation model whose accuracy is about 80 m, is 71 m. Three fringes are clearly observed nearby the epicentral area. Each cycle in the SAR interferogram corresponds to a ground movement of 28 mm in the line of sight. This allows to calculate the coseismic deformation, in slant range direction, by counting the number of interferometric fringes. The coseismic surface deformation corresponding to the observed concentric fringes is equal to 84 mm. The maximum deformation is observed in the inner fringe, which is the northern one and lies very close to the relocated epicenter of the mainshock. Kontoes *et al.* (2000) also used interferometric combinations of SAR images and calculated the coseismic deformation. They observed two fringes equivalent to 56 mm coseismic surface deformation and by modeling this deformation, they estimated a slip of 300 mm on a fault of 18 km length. The main difference between the two interferograms is the number of fringes, since at the presented one (Figure 5) the inner third fringe is clearly observed. This could be attributed to the different temporal separation, between the scenes of the two interferometric pairs. The seismic moment calculated in this study is 1.0 10^{25} dyn·cm, (rigidity $\mu = 3 \times 10^{11}$ dyn cm^{-1}). Taking into account fault dimensions equal to 15 $\times$ 10 km, the resulting slip is 220 mm, which is in agreement with the one proposed by Kontoes *et al.* (2000).

The location of the hypocenter combined with the differential interferogram (in SAR) together with the source duration and aftershock distribution suggests a source directivity to the east. In Figure 6 the recordings of the mainshock for the Sofi, Desf and Athu Cornet stations are presented. In all three stations an important phase is observed approximately 5 sec after the first P-arrival time in Desf and Sofi while in Athu at about 1.5 sec. No such phase was observed in any foreshock or aftershock and, therefore, it can not be attributed to the local structure of the seismogenic area. On the other hand, this phase can be explained as a source propagation effect. Taking into account the above observations we assume that this phase could be a stop phase caused by a barrier. Assuming that the distance between hypocenter and barrier is about $L = 10$ km, the rupture velocity is $V_r = 3$ km/sec and the wave propagation velocity is $V_p = 6.0$ km/sec, then the duration of rupture is $T_r = 3.3$ sec while the wave requires $T_p = 1.6$ sec to travel the same distance. This means that a Doppler phenomenon is in effect. The Athu station is azimuthally located along the direction of rupture propagation and the stop phase must be observed at $T_{sp} = T_r - T_p = 1.7$ sec. The Desf station is located on the opposite direction, therefore the stop phase must be observed at $T_{sp} = T_r + T_p = 4.9$ sec. Finally, the Sofi station at an almost perpendicular direction should perceive the stop phase at $T_{sp} = 4.5$ sec (the distance between the station and the barrier is the hypotenuse of the right triangle formed between the station, the barrier and the fault). Thus, the time difference between the first P-wave and the stop phase arrival times at each station must be in agreement with the directivity scenario, as it is the case.

For the majority of important earthquakes, it has been observed that the slip diminishes progressively during the rupture propagation until it stops. This does not seem to be the case for the Athens earthquake, since the rupture propagation stopped abruptly. Based on the above mentioned observations, we propose the following rupture process model: the rupture nucleated at the deep western edge of the fault plane and propagated eastward, until it stopped abruptly at the roots of Aegaleo Mountain. This means that the Aegaleo Mountain acted as a barrier

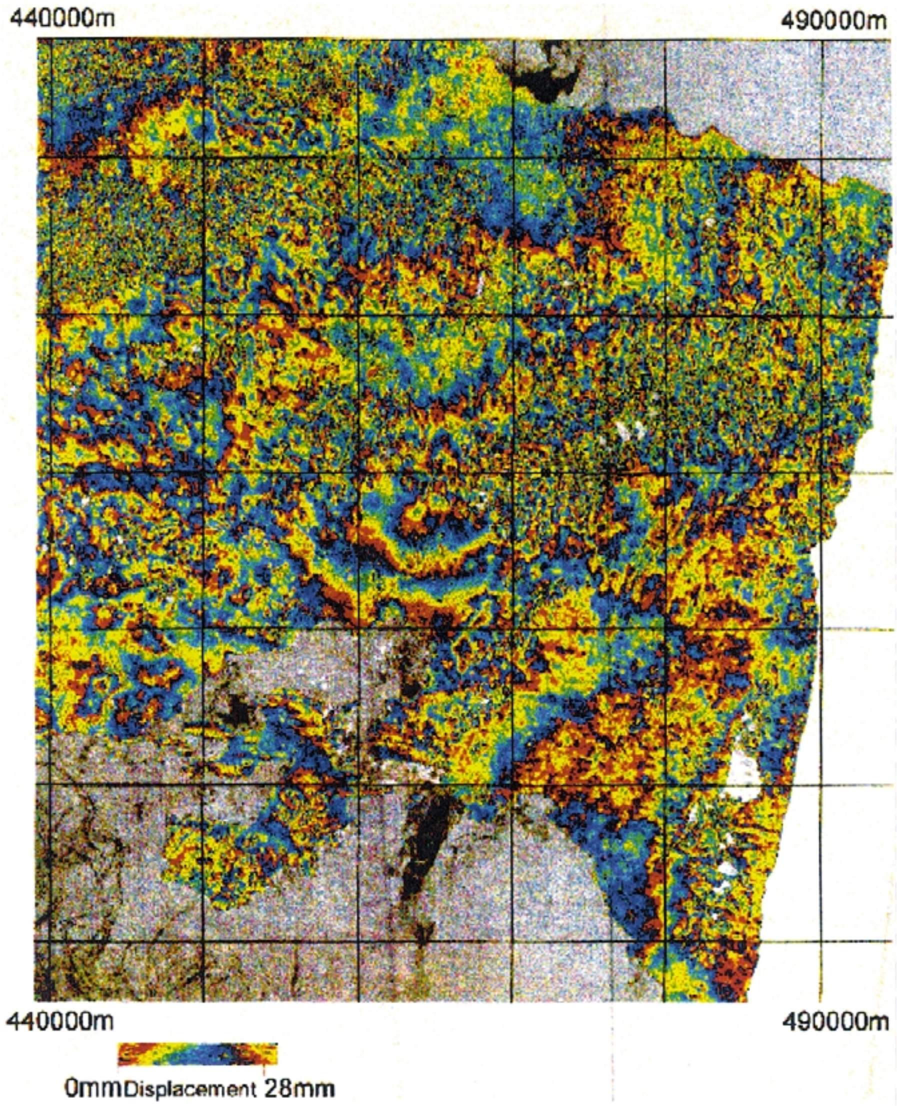

Figure 5. SAR differential interferogram.

that caused both an interference phenomenon and diffracted waves. This abrupt stopping can explain the big damage observed close to the eastern edge of the fault plane, as well as the concentration of the aftershocks in this area.

One day after the occurrence of the mainshock field reconnaissance was performed, but no surface breaks were observed, although the Parnitha normal fault clearly appears on satellite images. Only some small fissures striking N110° were observed at the Agios Kyprianos monastery and at the Fili castle (both in the vicinity of the Fili station). The length of the Parnitha fault is approximately 15 km

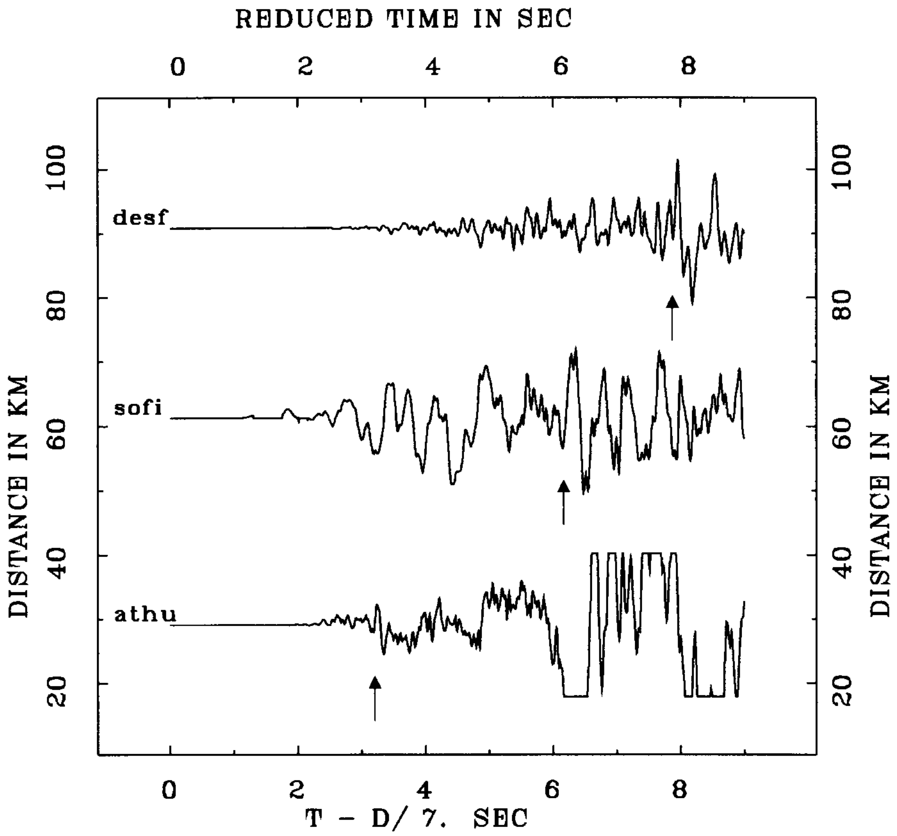

Figure 6. Recordings of the mainshock for the Sofi, Desf and Athu Cornet stations, where an important phase is observed in all three stations 5 sec after the first P-wave arrival time.

striking E–W, as it can also be noticed on satellite images, and dipping south. These observations are in agreement with the results obtained by body wave modeling that revealed normal faulting striking E–W and dipping south.

4. Aftershock Distribution and Fault Plane Solutions

The Geophysics Department of the Athens University started the installation of 6 digital 3 component continuous recording seismographs (FILI, STEF, MAGO, PSAR, NEOK and ZOFR) and 2 digital accelerographic instruments (PEFK, COUR) recording in trigger mode, 1 day after the mainshock (Figure 2). Network installation was based upon the first epicenter locations of the aftershock sequence provided by the CORNET network. Thus, sufficient geometrical and azimuthal distribution for both hypocenter location and focal mechanisms reliable determination was accomplished.

The array remained on site for a time period of about 4 months, until the end of December 1999 and recorded more than 3500 aftershocks. Initially, a total of 3668

Table III. Velocity model

Velocity (km/s)	Depth (km)
4.80	0.0
4.85	1.0
5.39	3.0
5.54	4.0
5.75	6.0
5.92	8.0
6.17	11.0
6.80	15.0
7.18	20.0
8.05	40.0

earthquakes were located within the field of acceptable uncertainties (ERZ, ERH, RMS) using the HYPO71 algorithm and a detailed 1-D velocity structure (Table III). The velocity structure, which improved the solutions compared to the starting model, was derived by the application of a method suggested by Kissling *et al.*, (1994, 1995) on a dataset of 500 selected earthquakes. The selection of the dataset depended on the number of P and S phase readings and the quality of the initial location. The large number of satisfactory locations (3668 events) allowed further filtering of the dataset with rather strict criteria, such as: number of Phases > 10, RMS < 0.1 s, ERH and ERZ < 1.0 km. The above selection yielded 1813 events for further investigation.

The aftershock distribution of the 1813 events (Figure 7) confines two principal clusters in the vicinity of PSAR (where the mainshock is located) and PEFK stations respectively, while in the area between the two clusters aftershock activity appears to be lower. Temporally, the majority of aftershocks of the west cluster precede those of the east, with the duration of the west cluster activity mainly restricted within the first 3 days of the sequence. The number of aftershocks of the east cluster is larger, while their spatial distribution appears more diffused. Furthermore, aftershocks of greater magnitude were also located in the eastern cluster while epicenters east of the Aegaleo mountain correspond to events that occurred later in the sequence.

The geometry of the network allowed reliable fault plane solution determinations of the aftershocks using the P-wave first motion polarities method. For a total of 1050 focal mechanisms, 356 were sufficiently constrained using more than 9 polarities. Most of these fault plane solutions indicate normal faulting. A small number of mechanisms corresponding to reverse and strike-slip faulting were also observed within the diffused eastern cluster. The majority of normal and oblique normal focal mechanisms indicate a WNW–ESE striking and south-dipping plane,

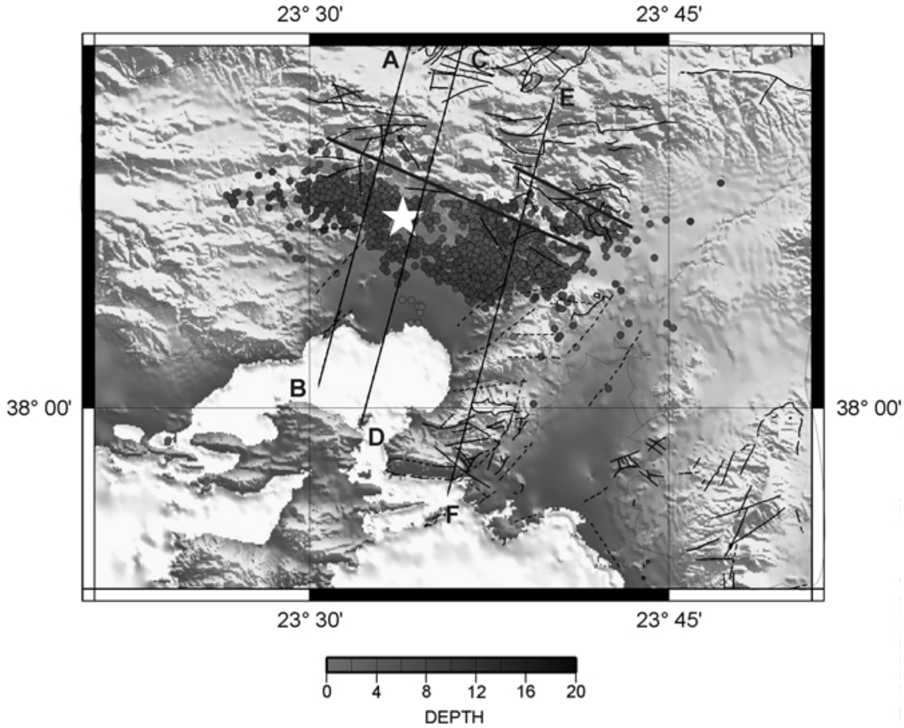

Figure 7. Location of selected aftershocks recorded by the local temporary network and cross-section directions. The star represents the epicenter of the mainshock.

consistent with the fault plane solution of the mainshock, determined by body-wave modeling. Due to the large number of calculated focal mechanisms, only the largest aftershocks ($M > 1.8$) are presented in Figure 8. In addition, rose diagrams of the P and T axes orientations of the well constrained fault plane solutions are presented in Figure 9. These diagrams indicate that the T axis is almost horizontal with a mean NNE–SSW orientation, while the P axis appears almost vertical.

Cross-sections along a NNE–SSW direction of a width of 2 km, reveal that most of the seismic activity appears to be located within a depth range 2–11 km and is mainly concentrated at a depth of 7 km (Figure 10). Similar focal depths were obtained by Papadopoulos *et al.* (2000) and Tselentis and Zahradnik (2000a, b). The lack of shallow activity between 0–2 km could also support the fact that the rupture did not reach the surface.

The first two cross-sections (Figure 10, sections A–B and C–D) clearly indicate a southwards dipping plane, an observation that is also confirmed by the focal mechanisms of the aftershocks. The upward extension of the southwards dipping plane defined by the aftershock distribution and the focal mechanism of the mainshock (Figure 10, section C–D) probably correlates with the Parnitha fault scarp mapped at the surface. In the same cross-section, a relative lack of activity around

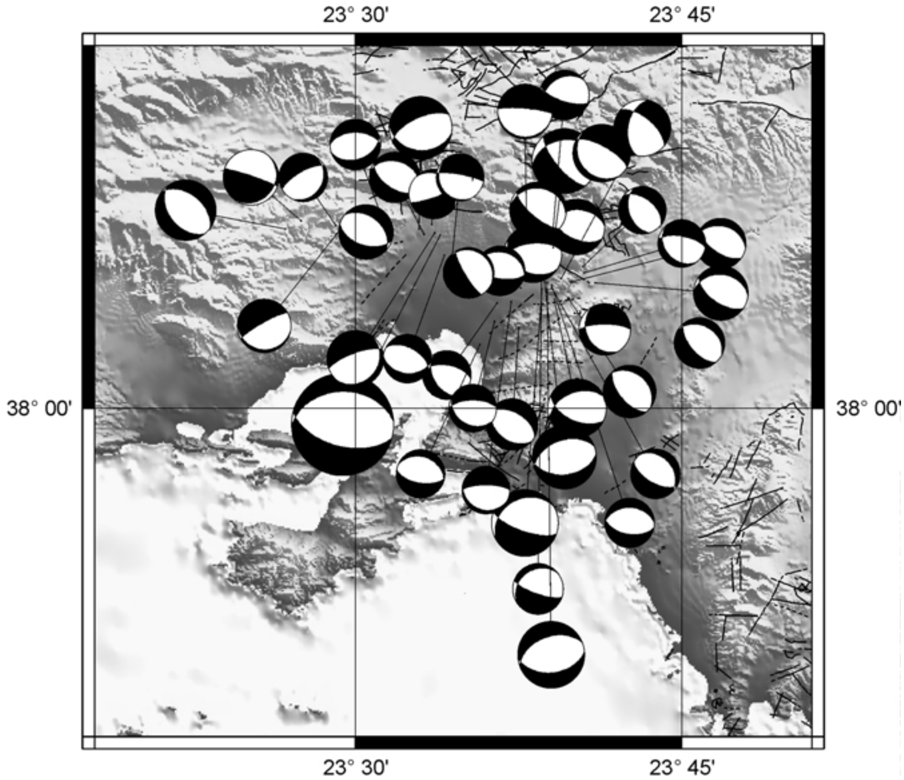

Figure 8. Selected fault plane solutions ($M_d > 1.8$) obtained by the local temporary network.

the depth of 8 km is revealed, as well as a clear change of the dip of the inferred fault plane.

In the same cross-section the distribution of the aftershocks located deeper than 8 km indicates a smoother dip angle while for those located higher than 8 km the dip angle becomes steeper. This aftershock distribution, which is independent of the selection criteria, is well defined by the aftershocks suggesting that this part of the fault is not dipping homogeneously as an evident change occurs at the 8 km depth. An alternative solution is to consider only the events located between 8 and 11 km and then to correlate these events with a possible fault to the north. However, this is probably not the case as the aftershock distribution located between 2 and 8 km can not be justified. This fault dip variation with depth has also been reported by Papadopoulos *et al*. (2000). It is also obvious that in cross-sections A–B and C–D of Figure 10 the aftershock distribution reveals that only one fault was activated in the west and central part of the seismogenic area. The cross-section E–F of Figure 10 indicates the complex mechanics of the earthquake sequence. At this part of the seismogenic area, the activation of Fili fault, situated north of the Parnitha fault (Figure 2), is also evident, as well as a small antithetic fault (Figure 11c).

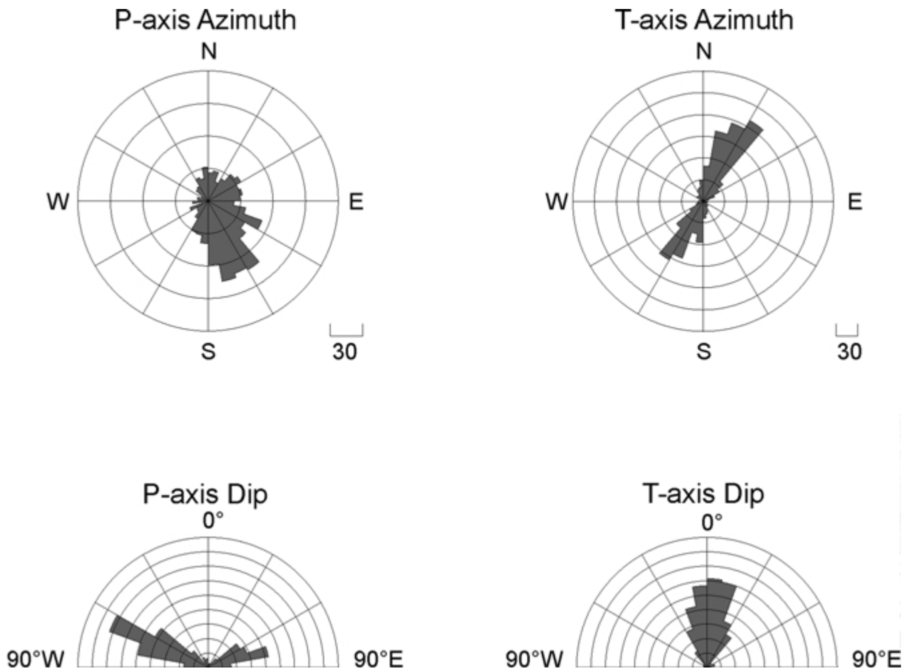

Figure 9. Rose diagrams of P and T axes azimuth orientation and dip of the 1050 constrained focal mechanisms.

This absence of hypocenters is clearly visible in Figure 11a, where the geometry of the fault becomes apparent in three dimensions. In the easternmost cross-section (Figure 10, section E–F), the spatial distribution of the hypocenters is diffused and no fault plane can be well defined. This fact can be attributed to the stress relaxation complexity procedure at the neighborhood of the main rupture termination. Nevertheless, two branches can be deduced that could possibly be related to the Parnitha main fault, noticed 1 in Figure 10, and Fili secondary fault, noticed 2 in Figure 10. The existence of the two branches can also be confirmed in Figure 11b. Moreover, the existence of a small quasi-antithetic fault can be deduced in the area between ZOFR and FILI stations in cross-section E–F noticed 3 in Figure 10, as well as from Figure 11b, c. The view angle of the diagram in Figure 11c has been chosen in order to demonstrate both the consistency of the aftershock distribution with the dip of the fault plane calculated for the mainshock and the existence of the quasi-antithetic fault.

Concluding, we propose that the main fault activated during the earthquake was the Parnitha fault. The eastward source propagation, discussed above, induced the activation of the Fili fault. Moreover, a small antithetic fault was activated during the sequence. Papadopoulos *et al*. (2000) propose the Fili fault as the main fault. This interpretation explains quite well the aftershock distribution 2 of the cross-section E–F of Figure 10, but cannot justify the distribution 1 in the same figure,

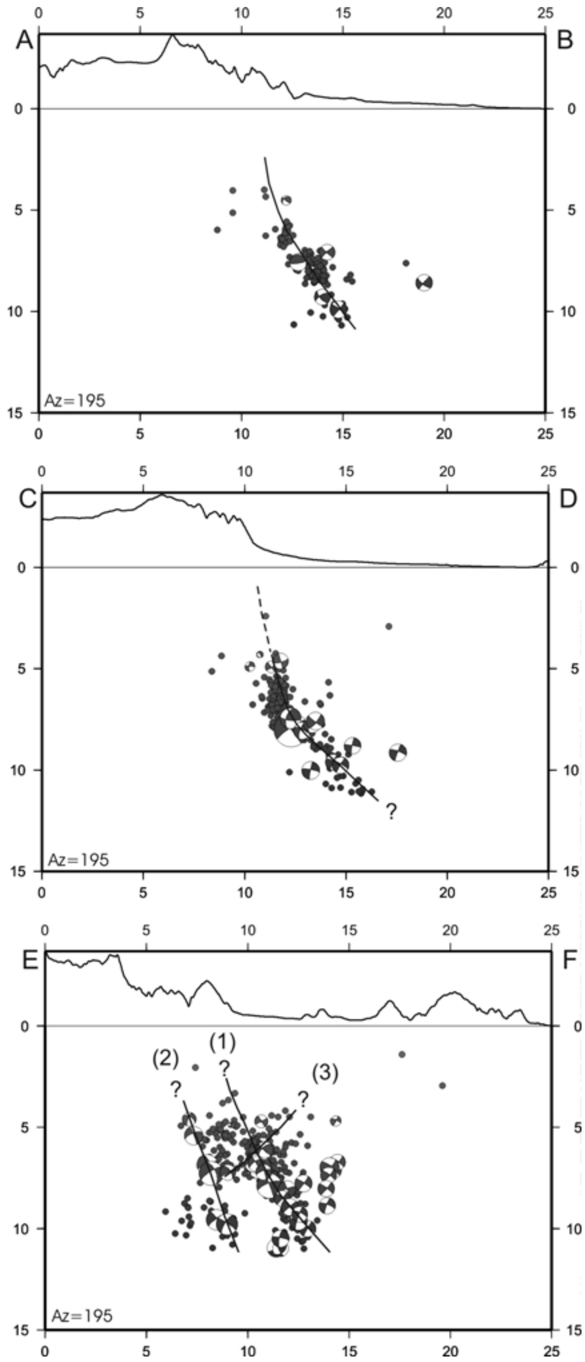

Figure 10. Three cross-sections along NNE–SSW azimuth from west to east, as indicated in Figure 7.

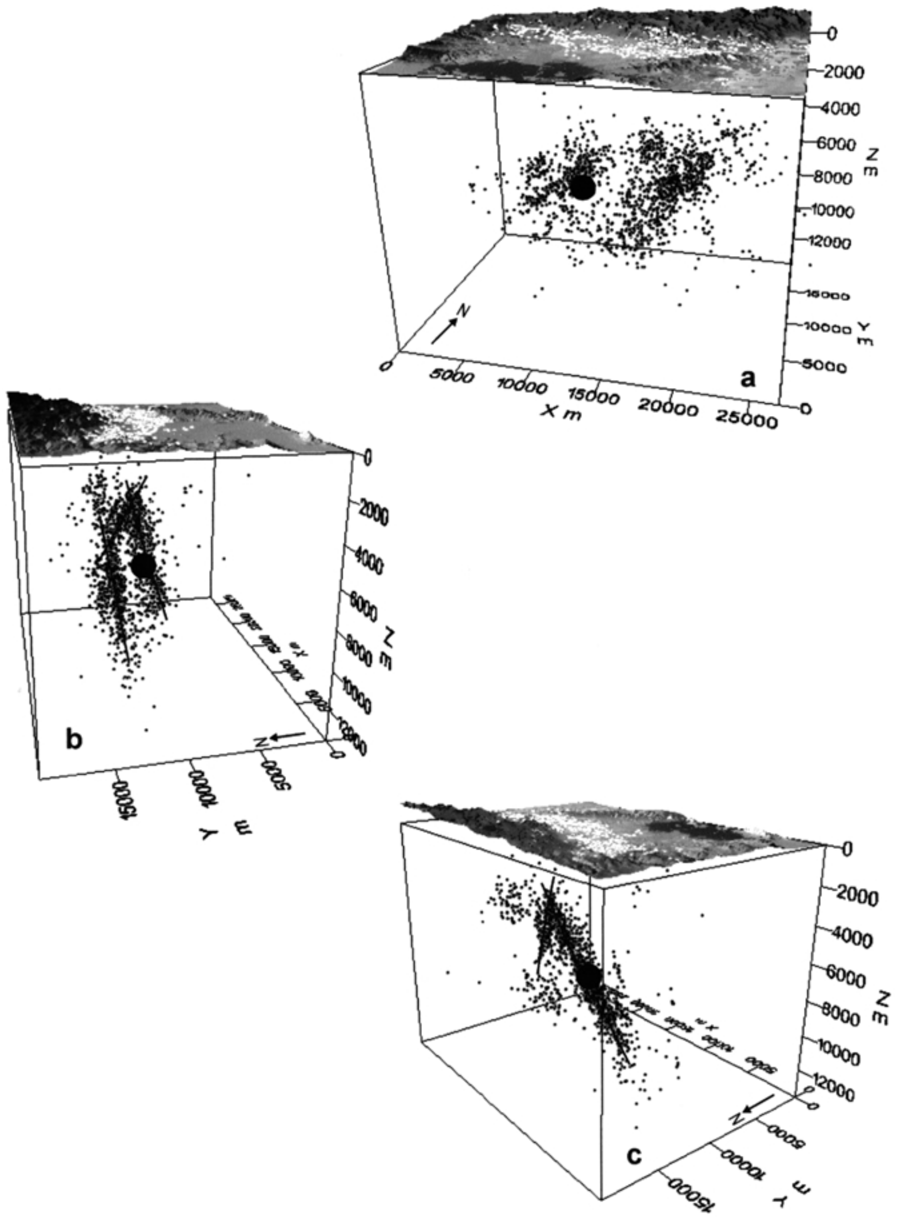

Figure 11. 3-D hypocentral distributions viewed along three different angles (vertical exaggeration 2 : 1). White points represent the epicenter distribution on the surface.

which is likely attributed to a fault plane located southern, the proposed Parnitha fault.

5. Conclusions

The Athens earthquake of 7 September 1999 occurred along the Parnitha normal fault, in a region of low seismicity. Seismological data, tectonic observations and SAR interferometry were used in order to study the source parameters, the rupture process and the aftershock sequence. Using local recordings, the mainshock was relocated at the deep western edge of the fault plane. The rupture nucleated at 38.105°N, 23.565°E, approximately 20 km NW of the city of Athens, at a focal depth of 8 km. The inner fringe of the differential interferometric image, that represents the highest deformation of the seismogenic area, verifies the relocated epicenter. The focal mechanism of the mainshock obtained by body wave modeling is: ($\phi = 105°$, $\delta = 55°$ and $\lambda = -80°$. The fault plane is striking in WNW–ESE direction dipping south and revealing an approximately N–S direction of extension. The direction of the main fault is similar to that of the eastern Corinthian Gulf major faults (Delibasis *et al.*, 2000). The calculated seismic moment is 1.0×10^{25} dyn·cm and the duration of the source time function 5 sec.

The detailed analysis of the aftershock sequence indicates that the seismic activity extends along the southern foothills of mount Parnitha. The depth distribution of the well-located aftershocks ranges between 2 and 11 km. At the central part of the fault zone, where the mainshock was located, low aftershock activity is observed. This fact could be attributed to the extensive stress release produced by the mainshock at this depth. Significant activity was triggered to the west, mostly within the first days of the aftershock sequence. The highest level of seismic activity was observed at the eastern part of the fault plane, where the spatial distribution was more diffused. Taking into account the aftershock distribution, tectonic observations and the duration of the source time function, the estimated fault area is 15×10 km^2.

Spatial distribution of aftershocks and focal mechanisms suggest a southwards dipping normal fault plane. No surface breaks were observed. Nevertheless, extrapolation of this fault plane, well-defined by the aftershock distribution, indicates that the fault trace at the surface corresponds to the Parnitha fault scarp. Most of the fault plane solutions, that were constrained using the P-wave first motion polarities, indicate normal faulting along E–W trending planes. Rose diagrams of the P and T axes indicate a pure extensional domain with a mean NNE–SSW orientation.

The rupture propagation of the Athens earthquake was characterized by a directivity effect to the east, as it was revealed by the azimuthal variation of the source time function duration and by a high-amplitude phase that was observed at the CORNET local stations. This phase was interpreted as a stop phase caused by the Aegaleo Mountain that acted as a barrier. This hypothesis is also supported by the aftershock spatial distribution, which was limited to the east by the Aegaleo

Mountain. The observed diffused pattern in this area could be associated to stress relaxation along minor local tectonic structures.

Acknowledgements

We are grateful to EPPO for providing the differential interferometric image and to Dr. I. Parcharidis for his support in interpreting it.

References

Armijo, R., Meyer, B., King, G., Rigo, A. and Papanastassiou, D.: 1996, Quaternary evolution of the Corinth rift and its implications for the late Cenozoic evolution of the Aegean, *Geophys. J. Int.* **126**, 11–53.

Bernard, P., Herrero, A., and Berge, C.: 1996, Modeling directivity of heterogeneous earthquake ruptures, *Bull. Seismol. Soc. Am.* **86**, 1149–1160.

Bernard, P., Briole, P., Meyer, B., Lyon-Caen, H., Gomez, J.-M., Tiberi, C., Berge, C., Cattin, R., Hatzfeld, D., Lachet, C., Lebrun, B., Deschamps, A., Courboulex, F., Larroque, C., Rigo, A., Massonet, D., Papadimitriou, P., Kassaras, J., Diagourtas, D., Makropoulos, K., Veis, G., Karakostas V., Papadimitriou, E., Papanastassiou, D., Chouliaras, G., and Stavrakakis, G.: 1997, The Ms = 6.2, June 15, 1995 Aigion earthquake (Greece): Evidence for low angle normal faulting in the Corinth rift, *J. Seismol.* **1**, 131–150.

Delibasis, N., Papadimitriou, P., Voulgaris, N., and Kassaras, I.: 2000, The Parnitha fault: Possible relationship with other neighboring faults and causes of larger damages, *Ann. Geol. Pays Hellen.* **XXXVIII**(B), 41–50.

Hatzfeld, D., Kementzetzidou, D., Karakostas, V., Ziazia, M., Nothard, S., Diagourtas, D., Deshamps, A., Karakaisis, G., Papadimitriou, P., Scordilis, M., Smith, R., Voulgaris, N., Kiratzi, A., Makropoulos, K., Bouin, M. P., and Bernard, P.: 1996, The Galaxidi earthquake of 18 November 1992: A possible asperity within the normal fault system of the Gulf of Corinth (Greece), *Bull. Seismol. Soc. Am.* **86**(6), 1987–1991.

Herrero, A. and Bernard, P.: 1994, A kinematic self-similar rupture process for earthquakes, *Bull. Seismol. Soc. Am.* **84**, 1216–1228.

Jackson, J. J., Gagnepain, J., Housema, G., King, G., Papadimitriou, P., Soufleris, P., and Virieux, J.: 1982, Seismicity, normal faulting and the geomorphological development of the Gulf of Corinth (Greece): The Corinth earthquakes of February and March 1981, *Earth Planet. Sci. Lett.* **57**, 377–397.

Kikuchi, M. and Kanamori, H.: 1982, Inversion of body waves, *Bull. Seismol. Soc. Am.* **72**, 491–506.

King, G. C. P., Ouyang, Z. X., Papadimitriou, P., Deschamps, A., Gagnepain, J., Houseman, G., Jackson, J. A., Soufleris, C., and Virieux, J.: 1985, The evolution of the Gulf of Corinth (Greece): An aftershock study of the 1981 earthquakes, *Geophys. J. R. astr. Soc.* **80**, 677–693.

Kissling, E., Ellsworth, W. L., Eberhart-Phillips, D., and Kradolfer, U.: 1994, Initial reference models in local earthquake tomography, *J. Geoph. Res.* **V99**, 19635–19646.

Kissling, E., Solarino, S., and Cattaneo, M.: 1995, Improved seismic velocity reference model from local earthquake data in Northwestern Italy, *Terra Nova* **7**, 528–534.

Kontoes, C., Elias, P., Sykioti, O, Briole, P., Remy, D., Sachpazi, M., Veis, G., and Kotsis, I.: 2000, Displacement field and fault model for the September 7, 1999 Athens earthquake inferred from ERS2 satellite radar interferometry, *Geophys. Res. Lett.* **27**(24), 3989–3992.

Lyon-Caen, H., Armijo, R., Drakopoulos, J., Baskoutas, J., Delibasis, N., Gaulon, R., Kouskouna, V., Latoussakis, J., Makropoulos, K., Papadimitriou, P., and Pedotti, G.: 1988, The 1986 Kalamata

(S. Peloponnesus) earthquake: detailed study of a normal fault, evidences for east-west extension in the Hellenic Arc, *J. Geophys. Res.* **93**, 14967–15000.

Papadimitriou, P., Kassaras, I., Rigo, A., Lyon-Caen, H., Hatzfeld, D., Makropoulos, K., and Drakopoulos, J.: 1994, Source parameters of large and small earthquakes in Corinth Gulf (C. Greece), *Proceedings of the XXIV General Assembly of ESC. Athens, Greece*, Vol. II, pp. 848–858.

Papadimitriou, P., Makropoulos, K., Kassaras, I., Kaviris, G., and Drakopoulos, J.: 1996. The Eastern Corinthian gulf (Greece) seismological telemetry network (CORNET). Book of abstracts, p. 1, XXV General Assembly of ESC, Reykjavik, Iceland.

Papadimitriou, P., Kaviris, G., Voulgaris, N., Kassaras, I., Delibasis, N., and Makropoulos, K.: 2000, The September 7, 1999 Athens earthquake sequence recorded by the Cornet network: Preliminary results of source parameters determination of the main shock, *Ann. Geol. Pays Hellen* **XXXVIII**(B), 29–39.

Papadopoulos, G., Drakatos, G., Papanastassiou, D., Kalogeras, I., and Stavrakakis, G.: 2000, Preliminary results about the catastrophic earthquake of 7 September 1999 in Athens, Greece, *Seismol. Res. Lett.* **71**, 318–329.

Papazachos, B. C., Comninakis, P. E., Papadimitriou, E. E., and Scordilis, E. M.: 1984, Properties of the February–March 1981 seismic sequence in the Alkionides Gulf of central Greece, *Annales Geophysicae* **2**, 537–544.

Rigo, A., Lyon-Caen, H., Armijo, Deschamps, A., Hatzfeld, D., Makropoulos, K., Papadimitriou, P., and Kassaras I.: 1996. A microseismicity study in the western part of the Gulf of Corinth (Greece): Implications for large-scale normal faulting mechanisms, *Geophys. J. Int.* **126**, 663–688.

Tselentis G.-A. and Zahradnik, J.: 2000a, The Athens earthquake of September 7, 1999, *Bull. Seismol. Soc. Am.* **90**, 1143–1160.

Tselentis G.-A. and Zahradnik, J.: 2000b, Aftershock Monitoring of the Athens Earthquake of 7 September 1999. *Seism. Res. Lett.* **71**, 330–337.

Voulgaris, N., Kassaras, I., Papadimitriou, P., and Delibasis, N.: 2000, Preliminary results of the Athens September 7, 1999 aftershock sequence, *Ann. Geol. Pays Hellen* **XXXVIII**(B), 51–62.